

SemanticCAP: Chromatin Accessibility Prediction Enhanced by Features Learning from a Language Model

Yikang Zhang, Xiaomin Chu, Yelu Jiang, Hongjie Wu and Lijun Quan

Abstract: A large number of inorganic and organic compounds are able to bind DNA and form complexes, among which drug-related molecules are important. Chromatin accessibility changes not only directly affects drug-DNA interactions, but also promote or inhibit the expression of critical genes associated with drug resistance by affecting the DNA binding capacity of TFs and transcriptional regulators. However, Biological experimental techniques for measuring it are expensive and time consuming. In recent years, several kinds of computational methods have been proposed to identify accessible regions of the genome. Existing computational models mostly ignore the contextual information of bases in gene sequences. To address these issues, we proposed a new solution named SemanticCAP. It introduces a gene language model which models the context of gene sequences, thus being able to provide an effective representation of a certain site in gene sequences. Basically, we merge the features provided by the gene language model into our chromatin accessibility model. During the process, we designed some methods to make feature fusion smoother. Compared with other systems under public benchmarks, our model proved to have better performance.

Keywords: chromatin accessibility; drug design; language model; transformer; feature fusion

1 Introduction

In human cells, genetic and regulatory information is stored in chromatin, which is deoxyribonucleic acid (DNA) wrapped around histones. Chromatin structure has a lot to do with gene transcription, protein synthesis, biochemical processes and other complex biological expressions. Among them, binding of small organic and inorganic molecules to DNA can influence numerous biological processes in which DNA participate. In particular, many anticancer, antibiotic, and antiviral drugs exert their primary biological effects by reversibly interacting with nucleic acids. Therefore, the study of its structure can help us design drugs to control gene expression and cure diseases (Aleksić and Kapetanović, 2014). Some regions of the chromatin are open to transcription factors (TFs), RNA polymers (RNAPs), drug molecules and other cellular materials, while others are tightly entangled together and do not play a part in most cellular processes. These two regions of the chromatin are called open regions and closed regions, which are also known as accessibility and inaccessibility separately (Wang et al., 2016). Measuring it can generate clues to gene function that help to identify appropriate targets for therapeutic intervention. Meanwhile, monitoring changes in chromatin accessibility can help track and understand drug effects. Gallon et al. (2021) find that chromatin accessibility changes at intergenic regions are associ-

ated with ovarian cancer drug resistance. Another example is the chromatin opening (increased accessibility) of the targeted DNA satellites can explain how DNA-binding pyrrole-imidazole compounds that target different *Drosophila melanogaster* satellites leading to gain- or loss-of-function phenotypes (Janssen et al., 2000). In recent years, many high-throughput sequencing technologies have been used for the detection of open regions, such as DNase-seq (Song and Crawford, 2010), FAIRE-seq (Simon et al., 2012) and ATAC-seq (Buenrostro et al., 2015). However, biological experimental methods are costly and time-consuming, thus cannot be applied to large-scale chemical examinations. These restrictions have promoted the development of calculation methods.

Alongside the progress in computer science, several kinds of sequence-based calculation methods have been proposed to identify functional regions. Simply we can divide them into traditional machine learning methods (Lee et al., 2011; Ghandi et al., 2014; Beer, 2017; Xu and Strick, 2021; Kumar and Bucher, 2016) and neural network methods (Alipanahi et al., 2015; Zhou and Troyanskaya, 2015; Min et al., 2017; Liu et al., 2018; Guo et al., 2020). Machine learning methods are mainly based on support vector machines (SVM). Lee et al. (2011) designed a SVM method based on k-mer features, which is defined as a segment of length k . This method recognizes enhancers in mammalian cells. Subsequently, the

gkm-SVM (gapped k-mers SVM) posed by Ghandi et al. (2014) exploited a feature set called interval k-mer features to improve the accuracy and stability of recognition. In recent years, with the rapid development of neural networks and the emergence of various deep learning models, a growing number of deep network models are used to solve such problems, where convolutional neural networks (CNNs) (Kalchbrenner et al., 2014) and recurrent neural networks (RNNs) (Hochreiter and Schmidhuber, 1997) dominate. DeepBind (Alipanahi et al., 2015) in 2015 and DeepSEA (Zhou and Troyanskaya, 2015) in 2017 got a significant performance improvement compared with traditional SVM-based methods after applying CNNs to modeling the sequence specificity of protein binding. Min et al. (2017) utilized the long short-term memory network (LSTM) to predict the chromatin accessibility and achieved state-of-the-art at the time, thus proving the effectiveness of RNNs for DNA sequence problems.

However, we point out that the previous methods have the following shortcomings at least. First, most of the previous methods are based on k-mer, that is, a segment of length k . Specifically, it takes a segment of length k at intervals. The artificial division of the original sequence may destroy the inside semantic information and cause difficulty in the learning of subsequent models. Second, with the progress of language models, we have the ability to learn the interior semantic information of sequences through pre-training. There have been related works in existed methods, such as Min et al. (2017) using Glove (Pennington et al., 2014) to train the word vectors of k-mer. However, these pre-train models are mostly traditional word vector methods. On the one hand, they can only learn the characteristics of the word itself and have no knowledge of the context of DNA sequences (Sun et al., 2019). On the other hand, they are limited to a specific dataset thus cannot be widely applied to other scenarios. Third, traditional CNNs and RNNs have been proved to be unsuitable for long-sequence problems (Bengio et al., 2013). CNNs restricted by the size of convolution kernels fail in learning global information effectively, while RNNs tend to cause gradient disappearance and slow training due to the lack of parallelizability when getting a long input. In contrast, the attention mechanism (Attention) (Vaswani et al., 2017) can effectively learn the long-range dependence of sequences, which has been widely used in the field of natural language processing.

In response to the above disadvantages, we constructed a chromatin accessibility prediction model based on features learning from a language

model. A implementation of our system is available at github.com/ykzhang0126/SemanticCAP. Our method has at least the following three improvements:

1. A DNA language model is utilized to learn the deep semantics of DNA sequences, and introduces the semantic features in the process of chromatin accessibility prediction. Therefore we obtain additional complex environmental information.
2. Both the DNA language model and the chromatin accessibility model use character-based input instead of k-mer which stand for segments of length k . The strategy prevents the information of original sequences from being destroyed.
3. The attention mechanism is widely used in our models in place of CNNs and RNNs, which can make the model more powerful and stable in handling long sequences.

Before formally introducing our method, we first present some preliminary knowledge, including some common sense information, theorems and corollaries.

2 Theories

Theorem 1. *For two standardized distributions using layer normalization (LN), which are denoted as X_1 and X_2 , the concat of them, that is, $X \equiv [X_1, X_2]$, is still a standardized distribution.*

Proof. Suppose that X_1 has n elements and X_2 has m elements. As we all know, LN (Ba et al., 2016) transforms the distribution X as

$$X \xrightarrow{\text{LN}} \frac{X - \mu}{\sigma} \quad (1)$$

where μ and σ are the expectation and standard deviation of X , respectively. Obviously, for the normalized distribution X_1 and X_2 , we have

$$E(X_1) = E(X_2) = 0 \quad (2)$$

$$D(X_1) = D(X_2) = 1 \quad (3)$$

where E stands for the expectation function and D stands for the deviation function. The new distribution X is derived by concatenating X_1 and X_2 , thus having $n + m$ elements. Inferring from Eq. 2, we get

$$E(X) = \frac{nE(X_1) + mE(X_2)}{n + m} = 0 \quad (4)$$

$$\begin{aligned} D(X) &= E(X^2) - E^2(X) = E(X^2) \\ &= \frac{nE(X_1^2) + mE(X_2^2)}{n + m} \end{aligned} \quad (5)$$

For X_1 and X_2 , we also know that

$$E(X_1^2) = D(X_1) + E^2(X_1) \quad (6)$$

$$E(X_2^2) = D(X_2) + E^2(X_2) \quad (7)$$

Substituting Eq. 2 and Eq. 3 into Eq. 6 and Eq. 7, and finally into Eq. 5, we get

$$D(X) = 1 \quad (8)$$

Eq. 4 and Eq. 8 demonstrate the standardization of X . \square

Theorem 2. *For any two distributions X_1, X_2 , there always exist two coefficients λ_1, λ_2 , so that the concat of them after being multiplied by the two coefficients respectively, that is $X \equiv [\lambda_1 X_1, \lambda_2 X_2]$, is a standardized distribution.*

Proof. Suppose that X_1 has n elements and X_2 has m elements. We denote the expectation of the two distributions as μ_1, μ_2 , and the variance as σ_1^2, σ_2^2 . Notice that λ_1 and λ_2 are all scalars. Now pay attention to X . To prove this theorem, we want X to be a standardized distribution, which requires the expectation of X to be 0 and the variance to be 1. Therefore, we can list the following equation set.

$$\begin{cases} E(X) = \frac{n\lambda_1 E(X_1) + m\lambda_2 E(X_2)}{n+m} = 0 \\ E(X^2) = \frac{nE((\lambda_1 X_1)^2) + mE((\lambda_2 X_2)^2)}{n+m} \\ D(X) = E(X^2) - E^2(X) = 1 \end{cases} \quad (9)$$

At the same time, we have equations similar to Eq. 6 and Eq. 7, that is

$$E((\lambda_1 X_1)^2) = D(\lambda_1 X_1) + E^2(\lambda_1 X_1) \quad (10)$$

$$E((\lambda_2 X_2)^2) = D(\lambda_2 X_2) + E^2(\lambda_2 X_2) \quad (11)$$

which is easy to calculate according to the nature of expectation and variance. Notice that Eq. 9 has two variables and two independent equations, meaning it should be solvable. By calculating Eq. 9, we can get the numeric solution of λ_1 and λ_2 as follows.

$$\begin{cases} \lambda_1^2 = \frac{m(n+m)\mu_2^2}{nm\mu_2^2(\mu_1^2 + \sigma_1^2) + n^2\mu_1^2(\mu_2^2 + \sigma_2^2)} \\ \lambda_2^2 = \frac{n(n+m)\mu_1^2}{nm\mu_1^2(\mu_2^2 + \sigma_2^2) + m^2\mu_2^2(\mu_1^2 + \sigma_1^2)} \end{cases} \quad (12)$$

The existence of Eq. 12 ends our proof. Actually, we get two sets of solutions here, for λ_1 can be either positive or negative, and so be λ_2 . The signs of λ_1 and λ_2 depend on the signs of μ_1 and μ_2 , which can be easily inferred from the first equation in Eq. 9. \square

Corollary 1. *For any distributions X_1, X_2, \dots, X_n , there always exist n coefficients $\lambda_1, \lambda_2, \dots, \lambda_n$, so that the concat of them after being multiplied by the n coefficients respectively, that is $X \equiv [\lambda_1 X_1, \lambda_2 X_2, \dots, \lambda_n X_n]$, is a standardized distribution.*

Proof. The overall proof way is similar to that in Theorem 2. Note that in this case, we have n variables but only 2 independent equations, resulting in infinite solutions according to Eq. 9. To be more precise, the degree of freedom of our solutions is $n - 2$. \square

Theorem 3. *In neural networks, for any two tensors X, Y which satisfy $E(X) = E(Y) = 0$, the probability of feature disappearance of X after concating and normalizing them is $\Omega(\frac{SD(Y)}{SD(X)})$, where SD represents the standard deviation.*

Proof. Feature disappearance is defined as a situation where the features are too small. Concretely, for a tensor X and a threshold t_{FD} , if the result of a subsequent operation of X is smaller than t_{FD} , the feature disappearance of X happens. Here t_{FD} can be an arbitrarily small value, such as 10^{-5} .

Suppose that X has n elements and Y has m elements. We denote the expectation of the two distributions as μ_1, μ_2 , and the variance as σ_1^2, σ_2^2 . As stated in the precondition, we already know

$$\mu_1 = \mu_2 = 0 \quad (13)$$

Let $Z \equiv [X, Y]$ and $Z' \equiv \text{LN}(Z) \equiv [X', Y']$. By the help of Eq. 9, we have

$$E(Z) = 0 \quad (14)$$

$$D(Z) = E(Z^2) = \frac{n\sigma_1^2 + m\sigma_2^2}{n+m} \quad (15)$$

We denote $E(Z)$ as μ and $D(Z)$ as σ^2 . According to Eq. 1, for X' we know that

$$E(X') = E\left(\frac{X - E(Z)}{\sqrt{D(Z)}}\right) = \frac{\mu_1 - \mu}{\sigma} \quad (16)$$

$$D(X') = D\left(\frac{X - E(Z)}{\sqrt{D(Z)}}\right) = \frac{\sigma_1^2}{\sigma^2} \quad (17)$$

We denote $E(X')$ as μ'_1 and $D(X')$ as $\sigma_1'^2$. Now we consider the result of a subsequent operation of X , which is $\sum_{i=1}^n \lambda_i X'_i$. This is very common in convolution, linear or attention layers. For the result, an observation is

$$\sum_{i=1}^n \lambda_i X'_i \leq \sum_{i=1}^n |\lambda_i| |X'_i| \leq \lambda_m \sum_{i=1}^n |X'_i| \quad (18)$$

where $\lambda_m = \max_{1 \leq i \leq n} |\lambda_i|$. For the convenience of analysis, all λ are set to 1. This will not bring loss of generality, because the value scaling from λ_m to 1 has no effect in the subsequent derivation. Here we denote $\sum X'$ as $S_{X'}$. According to the central limit theorem (Lindeberg-Lévy form) (Giné, 1983), we find that $S_{X'}$ obeys a normal distribution, that is

$$S_{X'} \sim \mathcal{N}(n\mu'_1, n\sigma_1'^2) \quad (19)$$

For a feature disappearance threshold t_{FD} , We want to figure out the probability of $|S_{X'}| < t_{FD}$. Denote this event as FD and we can get

$$\begin{aligned} P(FD) &= Pr\{|S_{X'}| < t_{FD}\} \\ &= Pr\left\{\left|\frac{S_{X'} - n\mu'_1}{\sqrt{n}\sigma_1'}\right| < \frac{t_{FD} - n\mu'_1}{\sqrt{n}\sigma_1'}\right\} \\ &= 2\Phi\left(\frac{t_{FD} - n\mu'_1}{\sqrt{n}\sigma_1'}\right) - 1 \end{aligned} \quad (20)$$

where Φ is the cumulative distribution function (cdf) of the standard normal distribution. Since it is an integral which does not have a closed form solution, we cannot directly analyze it. According to Eq. 13, Eq. 14 and Eq. 16, we know $\mu'_1 = 0$. At the same time we know that t_{FD} is a small number, leading to $\frac{t_{FD}}{\sqrt{n}\sigma_1'} \rightarrow 0$. Therefore, we have the equation as follows.

$$\begin{aligned} \Phi(x) &= \Phi(0) + \varphi(0)x + R_1(x) \\ &= 0.5 + \frac{1}{\sqrt{2\pi}}x + o(x) \end{aligned} \quad (21)$$

The formula is a Taylor expansion where φ is the probability density function (pdf) of the standard normal distribution, $R_1(x)$ is the Lagrange remainder and $o(x)$ is the Peano remainder standing for a high-order infinitesimal of x . Combining Eq. 15, Eq. 17, Eq. 20 and Eq. 21, we can get

$$\begin{aligned} P(FD) &= t_{FD} \sqrt{\frac{2(k_s k_d^2 + 1)}{\pi n(k_s + 1)}} + o(k_d) \\ &= \Omega(K_d) \end{aligned} \quad (22)$$

where $k_s = \frac{m}{n}$ and $k_d = \frac{\sigma_2}{\sigma_1}$. The above equation can also be written as $P(FD) = \Omega\left(\frac{SD(Y)}{SD(X)}\right)$. \square

Corollary 2. *In neural networks, feature disappearance can lead to gradient disappearance.*

Proof. According to Theorem 3, the feature disappearance happens if there exists a tensor T such that $|T| < t_{FD}$. Similar to the definition of feature disappearance, gradient disappearance is defined as a situation where the gradients are too small. Concretely,

for a parameter C with the gradient of $grad_C$ and a threshold t_{GD} , if $grad_C$ is smaller than t_{GD} , the gradient disappearance of C happens. Here t_{GD} can be an arbitrarily small value.

Consider a subsequent operation of T , which is $T' = CT^n$, where n stands for the number of layers involved in the calculation. The gradient disappearance happens if

$$|grad_C| = \left|\frac{dT'}{dC}\right| = |T^n| = |T|^n < t_{GD} \quad (23)$$

At the same time, we already have $|T|^n < t_{FD}^n$, which means we just need to meet

$$t_{FD}^n < t_{GD} \quad (24)$$

Note that t_{FD} is a small number, which means $t_{FD} < 1$. Finally we derive a formula of n .

$$n > \frac{\log t_{GD}}{\log t_{FD}} \quad (25)$$

Thereby we get a sufficient condition for n and we can come to a conclusion. The disappearance of gradients occurs in layers deep enough after the disappearance of features. \square

The above corollary is consistent with intuition. The disappearance of gradients is always accompanied by the disappearance of features, and it is always a problem in deep neural networks.

Theorem 4. *In neural networks, for any two tensors X_1, X_2 of the same dimension, there always exist two matrices M_1, M_2 , so that the operation of concating them and the operation of adding them after being multiplied in the Hadamard format by the two matrices respectively, are equivalent in effect.*

Proof. First of all, we illustrate the definition of Hadamard product (Horn, 1990). The Hadamard product (also known as the element-wise product) is a binary operation that takes two matrices of the same dimensions and produces another matrix of the same dimension. Concretely, we can define it as

$$\begin{aligned} A(R, N) \circ B(R, N) &= AB(R, N) \\ AB_{ij} &= A_{ij}B_{ij} \end{aligned} \quad (26)$$

The symbol ' \circ ' is used to distinguish from the more common matrix product, which is denoted as ' \cdot ' and usually be omitted. The definition implies that the dimension of X_1 should be the same as that of M_1 , so are X_2 and M_2 . At the same time X_1 and X_2 are assumed to have the same dimension in the precondition of our proposition. So we might as well set them

to $\mathbb{R}^{R \times N}$. Now we give the representation of X_1 and X_2 .

$$X_1 = \begin{pmatrix} p_1 \\ p_2 \\ \vdots \\ p_R \end{pmatrix} \quad X_2 = \begin{pmatrix} q_1 \\ q_2 \\ \vdots \\ q_R \end{pmatrix} \quad (27)$$

Our goal is to weigh the effect of the two operations. For the convenience of comparison, we let the results after the two operations multiply a matrix, thus converting the dimension to $\mathbb{R}^{R \times M}$. Adding a linear layer is very common in neural networks, and it hardly affects the network's expression ability.

Considering the first scheme, the concat of X_1 and X_2 , we have

$$\begin{aligned} U &= [X_1, X_2] \cdot A \\ &= \begin{pmatrix} p_1 & q_1 \\ p_2 & q_2 \\ \vdots & \vdots \\ p_R & q_R \end{pmatrix} (a_1 \quad a_2 \quad \dots \quad a_M) \end{aligned} \quad (28)$$

where $A \in \mathbb{R}^{2N \times M}$ and $U \in \mathbb{R}^{R \times M}$. Observing the i -th row and j -th column of U , we can find that

$$\begin{aligned} U_{ij} &= [p_i, q_i] \cdot a_j \\ &= [p_i, q_i] \cdot [a_{jp}, a_{jq}] \\ &= p_i \cdot a_{jp} + q_i \cdot a_{jq} \end{aligned} \quad (29)$$

Considering the second scheme, with the addition of X_1 and X_2 as the core, we have

$$\begin{aligned} V &= (M_1 \circ X_1 + M_2 \circ X_2) \cdot B \\ &= \begin{pmatrix} \lambda_{11} \circ p_1 + \lambda_{12} \circ q_1 \\ \lambda_{21} \circ p_2 + \lambda_{22} \circ q_2 \\ \vdots \\ \lambda_{R1} \circ p_R + \lambda_{R2} \circ q_R \end{pmatrix} (b_1 \quad b_2 \quad \dots \quad b_M) \end{aligned} \quad (30)$$

where $B \in \mathbb{R}^{N \times M}$ and $V \in \mathbb{R}^{R \times M}$. Still we pay attention to the i -th row and j -th column of V and find that

$$\begin{aligned} V_{ij} &= (\lambda_{i1} \circ p_i + \lambda_{i2} \circ q_i) \cdot b_j \\ &= \sum ((\lambda_{i1} \circ p_i + \lambda_{i2} \circ q_i) \circ b_j^T) \\ &= \sum (\lambda_{i1} \circ b_j^T \circ p_i + \lambda_{i2} \circ b_j^T \circ q_i) \\ &= \sum (\lambda_{i1} \circ b_j^T \circ p_i) + \sum (\lambda_{i2} \circ b_j^T \circ q_i) \\ &= p_i \cdot (\lambda_{i1} \circ b_j^T)^T + q_i \cdot (\lambda_{i2} \circ b_j^T)^T \\ &= p_i \cdot (\lambda_{i1}^T \circ b_j) + q_i \cdot (\lambda_{i2}^T \circ b_j) \end{aligned} \quad (31)$$

Comparing Eq. 29 and Eq. 31, we find that when we let $\lambda_{i1}^T \circ b_j$ equal to a_{jp} and $\lambda_{i2}^T \circ b_j$ equal to a_{jq} , the values of U and V are equal, which is a strong evidence of effect equivalence. \square

As the equivalence has been proved, the same as the plain concat no information is lost in the above method. We point out that the Hadamard product is an alternative version of the gate mechanism (Liu and Perez, 2017). We use coefficients to adjust the original distribution to screen out effective features. For the speed and stability of training, it is recommended to set the initial value of M to 1.

Further, we can observe the gradient of the parameters λ in Eq. 30, we have

$$\nabla \begin{pmatrix} \lambda_{11} \circ p_1 + \lambda_{12} \circ q_1 \\ \lambda_{21} \circ p_2 + \lambda_{22} \circ q_2 \\ \vdots \\ \lambda_{R1} \circ p_R + \lambda_{R2} \circ q_R \end{pmatrix} = \begin{pmatrix} p_1 & q_1 \\ p_2 & q_2 \\ \vdots & \vdots \\ p_R & q_R \end{pmatrix} \quad (32)$$

Compared with the gate mechanism, our method is simpler, space-saving, and more direct in gradient propagation.

Of course, Theorem 4 could be generalized to cases with arbitrary number of tensors. We describe it in the following corollary.

Corollary 3. *In neural networks, for any tensors X_1, X_2, \dots, X_n of the same dimension, there always exist n matrices M_1, M_2, \dots, M_n so that the operation of concatenating them and the operation of adding them after being multiplied in the Hadamard format by the n matrices respectively, are equivalent in effect.*

Proof. Similar to the proof of Theorem 4. \square

Theorem 5. *In neural networks, for a layer composed of n neurons, the effective training times of the neurons in this layer reach the maximum when the dropout rate is set to 0 or $1 - \frac{1}{n}$.*

Proof. The number of neurons in this layer is n , so we shall mark them as N_1, N_2, \dots, N_n . Suppose that the dropout rate (Baldi and Sadowski, 2013) is p and the total number of training times is t . We denote $1 - p$ as q .

Consider the t_i -th training. The network randomly selects nq neurons for update due to the existence of dropout mechanism. Denote these neurons as N_1, N_2, \dots, N_{nq} .

Without loss of generality, we consider the next time N_1 is selected, which is the t_2 -th training. We denote the number of neurons selected for update in N_2, \dots, N_{nq} as S , and the number of that selected in N_{nq+1}, \dots, N_n as T . Easily we know that the selection of neurons in S is an independent event, so we have

$$E(S) = q(nq - 1) \quad (33)$$

At the same time, the relationship between S and T is

$$T = nq - 1 - S \quad (34)$$

Inferring from Eq. 33 and Eq. 34, we get

$$E(T) = -nq^2 + nq + q - 1 \quad (35)$$

The neurons represented by S are the neurons that are updated jointly at time t_2 and time t_1 , thus belong to the same sub-network. We assume that they share one training gain with N_1 . At the same time, the neurons represented by T have not been updated at time t_1 , thus each of them has one unique training gain. Therefore, at the update time t_2 , the expected gain of N_1 is $1 \times \frac{1}{E(T)+1} \times \frac{1}{E(S)+1}$, which is derived from the above proportion analysis. Paying attention to t_1 and t_2 , we find that $t_2 - t_1$ obeys a geometric distribution, because the selection of N_1 is a Bernoulli experiment with probability q . That is $t_2 - t_1 \sim \mathcal{GE}(q)$, meaning that

$$E(t_2 - t_1) = \frac{1}{q} \quad (36)$$

Therefore, the expected number of training times of N_1 is $E(\frac{t}{t_2-t_1}) = tq$. The total training gain is the product of the number of training times and the gain of a single training, which we denote as G . Now the formula emerges.

$$G(q) = \frac{t}{-n^2q^3 + (n^2 + 2n)q^2 - (2n + 1)q + n + 1} \quad (37)$$

Denote $f(q)$ as the denominator of $G(q)$ and differentiate that to get

$$\frac{\partial f(q)}{\partial q} = -(nq - 1)(3nq - 2n - 1) \quad (38)$$

With the help of Eq. 38, it is easy to draw an image of $G(p)$ shown in Figure 1 where we set t to 1. The observation is that when $q = \frac{1}{n}$ or $q = 1$, that is, p is 0 or $1 - \frac{1}{n}$, G reaches the maximum value $\frac{t}{n}$, demonstrating the effective training times of N_1 are the largest. The conclusion can be generalized to every neuron in the layer. \square

Corollary 4. *In neural networks, if the amount of training data is sufficient, the optimal value of dropout rate is 0.5; if the amount of training data is insufficient, a number close to 1 is a better choice.*

Proof. Theorem 5 focuses on the effective training times of neurons in the network, and the corollary focuses on the representation ability. It can be seen from Eq. 37 that the effective training times of a certain layer is directly proportional to the total training

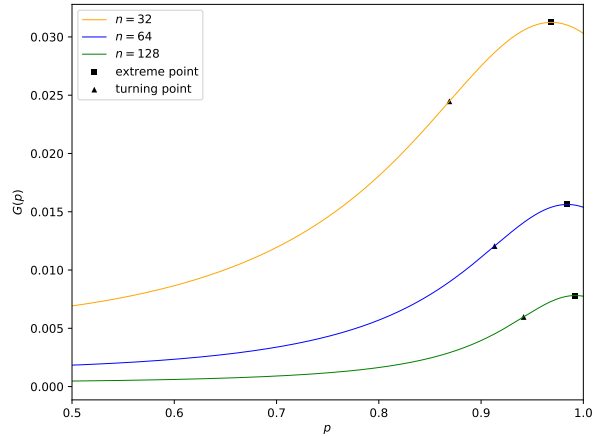


Figure 1: Gain curve as n differs. G varies with p , and the extreme points (squares) and turning points (triangles) vary with n . The turning point is approximately $8.72 \times 10^{-9}n^3 - 9.35 \times 10^{-6}n^2 + 2.44 \times 10^{-3}n + 0.78$, which is a good choice for the dropout rate.

times t . When the number of training times reaches a certain threshold, the network reaches a balance point, and further training will not bring any performance improvement.

If the training data are sufficient, which means t and G are large enough, the network is guaranteed to get fully trained. Therefore we do not need to worry about whether the training times of neurons in the network is enough. But we still need to consider the representation ability of the network, which has a close relationship with the number of sub-networks SN . It can be calculated as

$$SN = \binom{n}{n(1-p)} \quad (39)$$

which is a combination number. Obviously, when p is 0.5, the number of sub-networks is the largest, and the network's representation ability is relatively strong.

However, when the training data is not enough, we cannot guarantee the sufficiency of training. On the one hand, we need to set the dropout rate to a value close to 0 or $1 - \frac{1}{n}$ to guarantee the number of training as Theorem 5 says. On the other hand, in order to ensure the network's representation ability, we want the dropout rate be close to 0.5. Here a balanced approach is to choose the turning point shown in Figure 1, which considers both training times and representation ability. Because this point is difficult to analyze, we give a fitting function shown in Figure 1, whose error is bounded by 2×10^{-2} for n smaller than 512. \square

The above corollary is intuitive, because the complexity of the network should be proportional to the amount of data. Little data requires a simple model, calling for a higher dropout rate. Notice that a large dropout rate not only enables the model to be fully trained, but also helps to accelerate the process. In a modern neural network framework, the discarded neurons will not participate in the gradient propagation this time, which largely reduces the number of parameters need to be adjusted in the network.

3 Models

To address the task of chromatin accessibility prediction, we designed SemanticCAP, which includes a DNA language model shown in Section 3.1 and a chromatin accessibility model shown in Section 3.2. Briefly, we augment the chromatin accessibility model with features provided by the DNA language model, thereby improving the performance of chromatin accessibility prediction. The detailed methods are described below.

3.1 DNA language model

3.1.1 Process of data

We use the human reference genome GRCh37 (hg19) as the original data for our DNA language model. The human reference genome is a digital nucleic acid sequence database that can be used as a representative example of the gene set of an idealized individual of a species (Pan et al., 2019). Therefore, the model based on the database could be applied to various genetic-sequence-related issues.

The task we designed for our DNA language model is using context to predict the intermediate base. However, there are at least three challenges. First is that there are two inputs, the upstream and downstream, which are defined as the upper and lower sequence of a certain base. Since we predict the middle base from the information on both sides, the definition of the upstream and downstream are interchangeable, which means that the context should be treated in the same way. Second, the input is quite long, far from the length 4 of the output, which stands for the classification result of bases. The large gap between the input and output lengths leads to the fact that neural networks must be designed in a more subtle way, otherwise redundant calculations or poor results may occur. Third, we do not always have such long context data in real situations. For example, the length of upstreams in the DNA datasets in Table 1 mostly varies from 0 to 600, resulting in insufficient information in some cases.

To solve the above problems, we designed the simple but effective input format and training method.

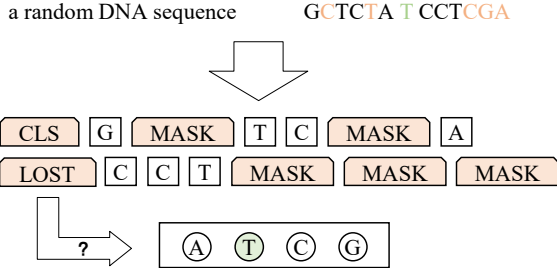


Figure 2: An example of mask operation on a random DNA sequence. Here, C and T of the upstream and CGA of the downstream are masked. The intermediate base is T, which is the target needs to be predicted.

First of all, we randomly select a certain position, taking the upstream and downstream sequence with a length of 512 as the input, and the output is the base connecting the upstream and downstream, i.e. A, T, C, G.

For the first challenge, we combine the upstream and downstream into one sequence, separated by a special prediction token [LOST], and provide different segment embeddings for the two parts. Also, a special classification token [CLS] is added to the beginning of the sequence to learn an overall representation of it. For the second challenge, the final hidden state corresponding to the token [LOST] is used as the aggregate sequence representation for classification tasks, by which the output dimension is reduced quickly without complex network structures. This technique was used in Bert (Devlin et al., 2018) for the first time. For the third challenge, some data augmentation tricks are applied in order to enhance the capabilities of the model. First, we can construct symmetric sequences based on the principle of base complementation and the non-directionality of DNA sequences, including the axial symmetry and mirror symmetry. This helps the model learn the two properties of DNA sequences. Second, we do not provide complete input to the model, which helps to enhance the model’s prediction ability under insufficient information. Basically, we mask some percentage of the input tokens at random, and concretely there are two strategies. For a certain sequence, either upstream or downstream, we mask (replace with [MASK]) 20% of random tokens in 10% of cases or 40% of consecutive tokens in 15% of cases. Figure 2 is an example below for our mask operation. In this case, 2 random tokens of the upstream and 3 consecutive tokens of the downstream are masked.

Finally, there is no need to worry about overfitting. First, we have 10^9 bases in the DNA dataset, mean-

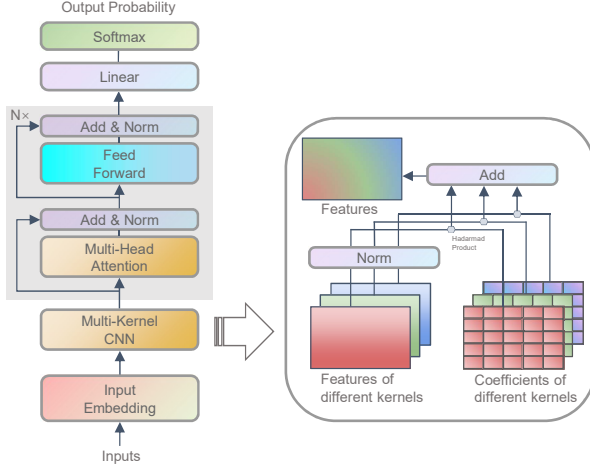


Figure 3: DNA language model. The part in the box on the right is our smooth feature addition (SFA).

ing that we will not over-learn some specific data. Second, we have mask and dropout operations in our training, which both are great ways to avoid over-training.

3.1.2 Model structure

The input and output are constructed as described in Section 3.1.1, and we denote them as T_{in} and T_{out} . Basically, the model can be described as

$$T_{in} \xrightarrow{\text{embed}} T_{embed} \xrightarrow{\text{multi-conv}} T_{cnns} \xrightarrow{\text{transformer}} T_{trans} \xrightarrow{\text{mlp}} T_{out} \quad (40)$$

where `embed` is the Input Embedding layer, `multi-conv` stands for our Multi-Kernel CNN, `transformer` represents the transformer blocks and `mlp` contains a Linear layer and a Softmax function. Figure 3 shows the full picture of the model.

`embed` is the encoding layer transforming the input sequence into a matrix. The dimension conversion is $\mathbb{N}^L \rightarrow \mathbb{R}^{L \times E}$, Where L is the length of the sequence and E is the encoding length. Specifically, we encode the input as

$$\begin{aligned} \text{embed}(T_{in}) = & \text{word} - \text{embed}(T_{in}) \\ & + \text{position} - \text{embed}(T_{in}) \\ & + \text{segment} - \text{embed}(T_{in}) \end{aligned} \quad (41)$$

where `word-embed` is the meaning of the word itself, `position-embed` provides the representation of different positions and `segment-embed` distinguishes the upstream and the downstream. An intuitive approach is concatenating the three encodings without loss of semantics. But this cost triple space. Instead,

we directly add these three encodings. This works because the three parameters are all leaf nodes of the training graph, which can automatically adapt to each other's distribution. By this way we reduce the dimension of the coded matrix, thus reducing the parameter space and data space.

`multi-conv` is the multi-kernel convolution layer learning a short-range relationship of the sequence. The dimension conversion is $\mathbb{R}^{L \times E} \rightarrow \mathbb{R}^{L \times H}$, where H is the hidden dimension. Here, we use convolution kernels of different lengths to learn local relationships at different distances, and propose a smooth feature addition (SFA) method to fuse these features. Specifically, we do

$$\text{multi-conv}(T_{embed}) = \sum_{i=0}^k \lambda_i \circ \text{LN}(\text{conv}_i(T_{embed})) \quad (42)$$

where `convi` is a normal one-dimensional convolution layer with a kernel length of l_i , whose output dimension is $\mathbb{R}^{L \times H}$, λ_i is a network parameter with a dimension of $\mathbb{R}^{L \times H}$ and k is the number of kernels of different lengths. The sizes of convolution kernels are small rather than large ones, whose advantages have been verified in DenseNet (Huang et al., 2017). On the one hand, small convolution kernels use less space than large convolution kernels. On the other hand, we need small convolution kernels to learn the local information of the sequence, while the long-range dependence of the sequence is to be explored by the subsequent transformer module.

Now we explain how we designed the smooth feature addition algorithm SFA. Before that, we have to take an insight into what happens in the plain concat of features.

In a sequence problem, we often directly concat two features in the last dimension. Specifically, if we have two features with dimensions $\mathbb{R}^{L \times M}$ and $\mathbb{R}^{L \times N}$, the dimension of the features after concat is $\mathbb{R}^{L \times (M+N)}$. We thought that this approach would not lose information, but in fact there is a danger of feature disappearance. For two features of different distributions learning from different modules, plain concat will bring an unbalanced distribution, where some values are extremely small. To make matters worse, layer normalization is usually used to adjust the distribution after a concat operation, making the values to be concentrated near 0. Quantitative analysis can be seen in Theorem 3. Finally, as the network goes deeper, the gradient disappears, leading to the difficulty of learning. This is proven in Corollary 2.

A naive thought is to normalize the two distributions before concatenating them, which proves to be correct in Theorem 1. However, it's not effective, for it

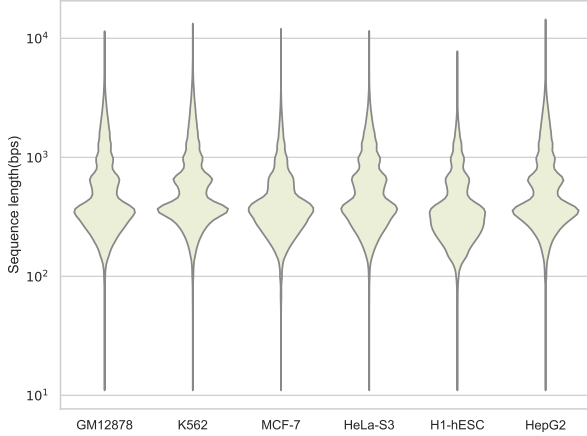


Figure 4: The length distribution of each cell, which is a more intuitive display of the content of the data. It can be seen that most of the lengths are concentrated between 10^2 - 10^3 .

converts the dimension from $\mathbb{R}^{L \times H}$ to $\mathbb{R}^{L \times kH}$, posing a challenge for the subsequent module design. Considering that the dimensions of convolution features are the same, inspiring us to find a way to smoothly add them using some tuning parameters. That’s how we designed SFA. Corollary 3 proves the equivalence of SFA and plain concat, and illustrates the working mechanism of SFA and its advantages in space occupation, feature selection and gradient propagation.

transformer is the stack of transformer blocks learning a long-range relationship of the sequence. The dimension conversion is $\mathbb{R}^{L \times H} \rightarrow \mathbb{R}^{L \times kH}$. Simply it can be described as

$$\text{transformer}(T_{cnns}) = \text{sub}(\text{ff}, \text{sub}(\text{attention}, T_{cnns})) \quad (43)$$

where $\text{sub}(f, x) = \text{LN}(x + f(x))$. ff represents the feed forward function and attention is short for multi-head attention. The module is proposed by Vaswani et al. (2017).

mlp is the output layer, responsible for converting the hidden state to the output. The dimension conversion is $\mathbb{R}^{L \times H} \rightarrow \mathbb{N}$. We extract the tensor corresponding to the token [LOST], convert it into an output probability through a linear layer, and generate the prediction value via a softmax function. The output process is

$$\text{mlp}(T_{trans}) = \text{softmax}(\text{linear}(T_{trans}['\text{[LOST]'}])) \quad (44)$$

3.2 Chromatin accessibility model

3.2.1 Process of data

We select DNase-seq experiment data of six typical cell lines as the original data for our chromatin accessibility model, including GM12878, K562, MCF-7, HeLa-S3, H1-hESC and HepG2. GM12878 is a type of lymphoblast, produced by EBV transformation from the blood of a female donor of Northern European and Western European descent. K562 is an immortalized cell derived from a female patient with chronic myeloid leukemia (CML). MCF-7 is a breast cancer cell sampled from a white female. HeLa-S3 is an immortal cell derived from a cervical cancer patient. H1-hESC is a human embryonic stem cell. HepG2 comes from a male liver cancer patient.

For each cell type, we downloaded the original sequence data from the ENCODE website, use a short read aligner tool bowtie (de Ruijter and Guldenmund, 2016) to map the DNA sequence to the human reference genome (hg19), and use HOTSPOT (John et al., 2011) to identify chromatin accessibility regions (peaks). We treat these variable-length sequences as positive samples. At the same time, we sample the same number and same size sequences from the whole genome as negative samples. An overview of the data is shown in Table 1, which shows the number of sequences, the minimum value, the median value, the maximum value and the standard deviation of lengths. Also, the distribution statistics of different datasets are shown in Figure 4. For the fairness of comparison, we removed sequences with length less than 36. We truncate or expand each sequence symmetrically to a sequence of length 768, and take a context of length 512 for each site in it. Similar to our DNA language model, a special classification token [CLS] is added to the beginning of the sequence to predict the accessibility. Therefore the actual input length of our model is $768 + 512 \times 2 + 1 = 1793$. From Figure 4, we observe that most of the lengths are clustered between 36 and 1792. This proves that our cut-off has little impact and is reasonable. Compared with the input length 800 in Min et al. (2017), our prediction length has increased by 124%, and the quantity of DNA sequences that do not need to be truncated in the original dataset has increased by 17.4%. Moreover, we do not pay a great price for such a long input because our context is handed over to a pre-trained model to predict. The output is the accessibility of the input sequence, i.e., either 0 for inaccessibility or 1 for accessibility.

Finally, the ratio of our training set, validation set, and test set is 0.85 : 0.05 : 0.10. The training set is used to train the model, the validation set is used

Table 1: An overall view of accessible DNA segments of each cell. l_mean and l_med show the approximate length of the data and l_std describes how discrete the data are. The unit of all length is bp.

Cell type	Code	Size	l_min	l_max	l_mean	l_med	l_std
GM12878	ENCSR0000EMT	244692	36	11481	610	381	614
K562	ENCSR0000EPC	418624	36	13307	675	423	671
MCF-7	ENCSR0000EPH	503816	36	12041	471	361	391
HeLa-S3	ENCSR0000ENO	264264	36	11557	615	420	524
H1-hESC	ENCSR0000EMU	266868	36	7795	430	320	347
HepG2	ENCSR0000ENP	283148	36	14425	652	406	626

to adjust the hyperparameters to prevent overfitting, and the test set is used to test the performance of the final model.

3.2.2 Model structure

The input and output are constructed as described in Section 3.2.1, and we denote them as T_{in} and T_{out} . Basically, the model can be described as

$$\begin{aligned}
 T_{in} &\xrightarrow{\text{embed}} T_{embed} \xrightarrow{\text{multi-conv}} T_{cnns} \xrightarrow{\text{sconcat}} T_{sconcat} \\
 &\xrightarrow{\text{transformer}} T_{trans} \xrightarrow{\text{mlp}} T_{out}
 \end{aligned}
 \tag{45}$$

where `embed` is the Input Embedding layer, `multi-conv` stands for our Multi-Kernel CNN, `sconcat` is short for our SConcat module, `transformer` represents the transformer blocks and `mlp` contains a Linear layer and a Sigmoid function. Figure 5 shows the full picture of the model. You may find that the accessibility model is very similar to our DNA language model. Indeed, we only modify some of the model structures and change the hyperparameters, but they are all very critical adjustments which make the model suitable for the task.

`embed` is the encoding layer transforming the input sequence into a feature matrix. The dimension conversion is $\mathbb{N}^L \rightarrow \mathbb{R}^{L \times E}$, Where L is the length of the sequence and E is the encoding length. Specifically, we encode the input as

$$\begin{aligned}
 \text{embed}(T_{in}) = &\text{word} - \text{embed}(T_{in}) \\
 &+ \text{position} - \text{embed}(T_{in})
 \end{aligned}
 \tag{46}$$

Note that there is no `segment-embed` in this task because there is no need to distinguish different segments.

`multi-conv` has been explained in Section 3.1.2. The dimension conversion is $\mathbb{R}^{L \times E} \rightarrow \mathbb{R}^{L \times G}$, where G is the dimension of features learning from this layer.

`sconcat` is the concat layer which fuses the features of the language model with the features learned from `multi-conv`. The dimension conversion is $\mathbb{R}^{L \times G} \rightarrow$

$\mathbb{R}^{L \times (G+H)}$, where H is the dimension of features generated from the DNA language model. Basically, we use the language model to construct features for sites in the sequence, and propose a smooth feature concat (SFC) method to fuse them with the previous features. What we do is

$$\text{sconcat}(T_{in}, T_{cnns}) = \text{LN}([\lambda_1 \circ \text{LM}(\overleftrightarrow{T_{in}}), \lambda_2 \circ T_{cnns}])
 \tag{47}$$

where $\overleftrightarrow{T_{in}}$ stands for the context of sites in T_{in} , λ_1 and λ_2 are two network parameters with a dimension of \mathbb{R}^L and `LM` refers to our DNA language model. Here, it receives a DNA sequence, then constructs the context for each site in the sequence and produces an output of length H . Specifically, if the length of the sequence is L , it will construct L pairs of context as the input and output a $\mathbb{R}^{L \times H}$ matrix.

Now we explain how we designed the smooth feature concat algorithm SFC. First, we have to mention that the output dimension of the language model is $\mathbb{R}^{L \times H}$ and the dimension of T_{cnns} is $\mathbb{R}^{L \times G}$, which means we cannot directly apply SFA in this scenario.

Fortunately, the analysis in Section 3.1.2 has already given a solution. We can normalize the two distributions separately before concatenating them. However, this method uses LN twice and consumes additional parameter space and data space. One doubt is that is it possible to use LN only once? The answer is yes. Theorem 2 states that for any two distributions, there always exist two coefficients, so that the concat after they are multiplied by these two coefficients is a standardized distribution. That's how our SFA works. We multiply the two tensors by two coefficients, and then do layer normalization after the concat of them. Thereby, we fuse the two features smoothly with only one LN operation. Interestingly, this method is a weakened version of Theorem 4.

`transformer` is the same as that described in Section 3.1.2. The dimension conversion is $\mathbb{R}^{L \times F} \rightarrow \mathbb{R}^{L \times F}$ where $F = G + H$.

`mlp` is the output layer, responsible for transforming the hidden state to the output. The dimension

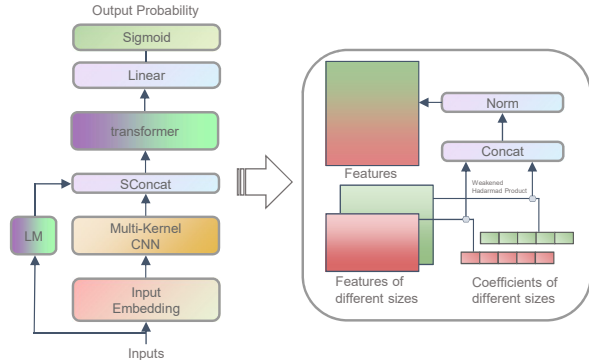


Figure 5: Chromatin accessibility model. The part in the box on the right is our smooth feature concat (SFC).

conversion is $\mathbb{R}^{L \times F} \rightarrow \mathbb{N}$. We extract the tensor corresponding to the token [CLS], convert it into an output probability through a linear layer, and generate the prediction value via a sigmoid function. The output process is

$$\text{mlp}(T_{trans}) = \text{sigmoid}(\text{linear}(T_{trans}['[CLS]'])) \quad (48)$$

4 Results and Discussions

4.1 SemanticDNA evaluation

We compared the performance of our proposed method with several baseline methods, including the gkmSVM (Ghandi et al., 2014), DeepSEA (Zhou and Troyanskaya, 2015) and kmer (Min et al., 2017). For the sake of fairness, all parameters were set as default. Besides, to prove the effectiveness of the DNA language model, we also tested our accessibility model excluding the DNA language model. For evaluation purpose, we computed two often-used measures, the area under the receiver operating characteristic curve (auROC) and the area under the precision-recall curve (auPRC), which are good indicators of the robustness of a prediction model. The classification results on six datasets are shown in Table 2. Compared to the best baseline kmer, our system has a maximum 1.25% improvement in auROC, and a maximum 2.41% improvement in auPRC. Although some results on some datasets are not good, our model outperforms kmer on average, with 0.02% higher auROC score and 0.1% higher auPRC score. Compared to gkmSVM and DeepSEA, SemanticCAP has an about 2%-3% improvement on average. Finally, the introduction of our DNA language model brings about a 2% performance improvement.

We also tested the accessibility prediction accuracy of loci shared in different cell lines. For example,

GM12878 and HeLa-S3 have 20 common loci, and the prediction accuracy of these 20 loci in both cell lines is 85% and 90%. Another example is that K562 and MCF-7 have 21 common loci, and the prediction accuracy is 80.9% and 90.5%, respectively. This shows the applicability of our system on the common loci between different cell lines.

4.2 Analysis of models

4.2.1 Effectiveness of our DNA language model

We did experiments on several different DNA language model structures, which can be roughly divided into two categories. The first category can be attributed to methods based on normal CNNs and the second uses our multi-conv architecture with data augmentation. Six structures are tested. At the same time, in order to test the prediction ability of different models in the case of insufficient information, we randomly masked some words and test the results. Complete results are shown in Table 3. Through the comparison of LSTM and Attention, we can find that the attention mechanism can greatly improve the prediction ability of the DNA language model. When using the MaxPooling and ReLU functions, we observed that the output of the last hidden layer is mostly 0, where the number of effective (not zero) neurons is about 3/256. This is because the ReLU function shields neurons whose values are less than 0, and MaxPooling selectively updates specific neurons. Therefore, we replace the MaxPooling with the AveragePooling, and the Attention layer that uses the ReLU function is replaced with a transformer. That's the third method in Table 3. The second category uses multi-conv to extract local features of the sequence. The introduction to multi-conv mechanism with data augmentation strategies brings increase in accuracy, especially when we mask some tokens. There are three kinds of feature fusion strategies: plain concat (PC), plain add (PA) and our smooth feature add (SFA). The third, fourth, and fifth items in the table indicate that SFA outperforms the other two fusion methods. The last item in Table 3, mconv(SFA)+trans, is the model we finally chose as our DNA language model.

4.2.2 Effectiveness of our chromatin accessibility model

We experimented with several chromatin accessibility model structures, which are all based on the transformer. The main difference is the use of multi-conv and the modules after the transformer. Complete comparison results are shown in Table 4.

First focus on the module before the transformer. We notice that the introduction of multi-conv also

Table 2: The result of chromatin accessibility prediction system comparative experiment. The code name of these datasets can refer to Table 1.

System	MT	PC	PH	NO	MU	NP	Average
(a) auROC							
gkmSVM	0.8528	0.8203	0.8967	0.8648	0.8983	0.8359	0.8697
DeepSEA	0.8788	0.8629	0.9200	0.8903	0.8827	0.8609	0.8782
kmer	0.8830	0.8809	0.9212	0.9016	0.9097	0.8722	0.8975
no feature ¹	0.8727	0.8664	0.9058	0.8840	0.8849	0.8699	0.8806
SemanticCAP	0.8907	0.8883	0.9241	0.9001	0.8982	0.8847	0.8977
(b) auPRC							
gkmSVM	0.8442	0.8081	0.8860	0.8627	0.8823	0.8123	0.8504
DeepSEA	0.8758	0.8551	0.9146	0.8888	0.8705	0.8508	0.8801
kmer	0.8774	0.8732	0.9156	0.8992	0.8968	0.8630	0.8973
no feature	0.8745	0.8663	0.9053	0.8852	0.8878	0.8730	0.8820
SemanticCAP	0.8914	0.8896	0.9218	0.9004	0.8993	0.8871	0.8983

¹ no feature is SemanticCAP without pre-train features.

Table 3: The result of DNA language model comparative experiment.

Model	Loss (no mask)	Accuracy (no mask)	Accuracy (mask 30%)
convs(max)+lstm	1.152	0.4538	0.3265
convs(max)+attention(relu)	1.113	0.4814	0.3687
convs(avg)+trans ¹	1.096	0.4926	0.3599
mconv ² (PC ³)+trans	0.968	0.5114	0.4572
mconv(PA ³)+trans	0.931	0.5187	0.4784
mconv(SFA ³)+trans	0.921	0.5202	0.4793

¹ trans refers to transformer+linear.

² mconv stands for our multi-conv layer.

³ PA is plain add, PC is plain concat and SFA is our smooth feature addition method.

Table 4: The result of chromatin accessibility model comparative experiment.

Model	Parameters (M)	Total (h)	auROC	auPRC	F1
PC+trans ¹ +lstm	4.16	4.6	0.8595	0.8625	0.7880
PC+trans+conv+lstm	4.95	2.9	0.8741	0.8765	0.8036
PC+trans+flatten	16.4	2.0	0.8822	0.8839	0.8124
PC+trans+conv+flatten	6.13	2.8	0.8817	0.8834	0.8119
PC+trans+linear	3.84	1.5	0.8839	0.8854	0.8144
mconv+PC+trans+linear	5.61	2.5	0.8881	0.8902	0.8590
mconv+SFC ² +trans +linear	5.61	2.5	0.8907	0.8914	0.8606

¹ trans is short for transformer blocks.

² SFC is our smooth feature concat method.

brought performance improvements, especially in F1. In our chromatin accessibility model, we concat the features provided by the DNA language model, where we can either directly concat (PC) them or using our SFC method. The evaluation values of the last two items show the superiority of SFC.

Now turn to the comparison of modules after the transformer. The transformation from the features of transformer to the result is a challenge. In this part, five methods are tested. Mention that `mconv+SFC+trans+linear` is the final model. In terms of training time, our model can be fully parallelized, which is more advantageous than LSTM based on recurrent networks. At the same time, our model has fewer parameters and a simpler structure than Flatten after CNNs, thus can converge quickly. In terms of evaluation, LSTM-based methods perform poorly, and the main reason is that it is difficult for LSTM to learn the long-range dependence of a sequence. The convolution layer improves the performance of the LSTM to some extent by shortening the sequence length. In methods based on Flatten, the introduction of convolution layers actually reduces the accuracy. Maybe it’s because that the convolution layers destroy the sequence features learned from the transformer. During multiple chromatin accessibility models, the method using mult-conv and our smoother concat method SFC obtain the best results with relatively small number of parameters.

4.3 Analysis of [CLS]

We can observe the effectiveness of introducing the [CLS] symbol in our accessibility model. A direct indicator is the feature corresponding to [CLS] after the transformer layer, i.e., the value of $T_{trans}['[CLS]']$ in Eq. 48. We randomly selected a certain number of positive and negative samples and use our chromatin accessibility model to predict them. For each sample, we output the 256-dimensional tensor corresponding to [CLS] after the transformer layer, and reduced it to two-dimensional space with t-SNE, which is shown in Figure 6. According to it, the feature has an ability to distinguish positive and negative examples, which is strong evidence of its effectiveness.

4.4 Analysis of SFA and SFC

In this part we did two comparison experiments of PA, PC, SFA and SFC.

In the experiment of various DNA language models, we made a comparison between SFA, PA and PC, corresponding to the last three items in Table 3. We used 5×10^6 samples to train the three models, drew the training loss map of them and saw what would happen, which is shown in Figure 7a. PA quickly re-

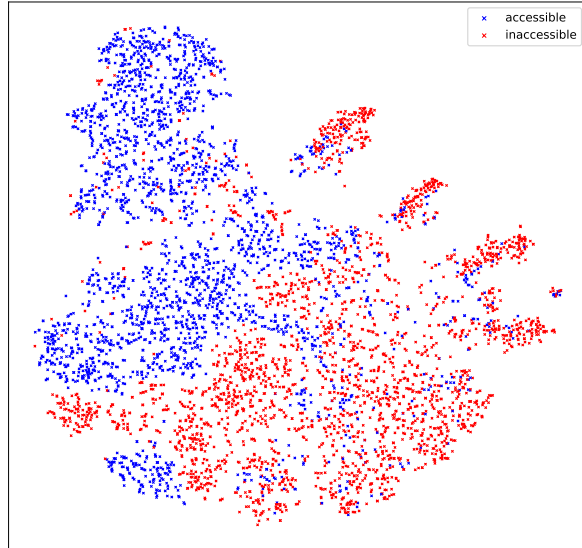


Figure 6: Features corresponding to the token [CLS] after the transformer for different samples. Accessible points and inaccessible points can be roughly distinguished.

duces the loss at the fastest speed at the beginning, because all features in multi-conv are trained at the same time to the same degree. But in the later stage, there appears a phenomenon that some features are overtrained, while others are not, leading to the oscillation of loss.

In the experiment of various chromatin accessibility models, we made a comparison between SFC and PC, corresponding to the last two items in Table 4. The first 5×10^3 samples are used to measure its training state, which is shown in Figure 7b. According to that, PC has a lower training speed, for it has a problem of gradient disappearance. Compared to it, the gradient propagation of SFA is selective and more stable for the whole term.

We can observe the effectiveness of SFA from another angle. Pay attention to the parameters C_{SFA} of SFA in multi-conv, whose dimension is $\mathbb{R}^{K \times L \times H}$, where K is the number of kernels, L is the sequence length and H is the hidden dimension. We normalized it and converted it to C'_{SFA} , whose dimension is $\mathbb{R}^{K \times L}$. We do this for both the language model and the chromatin accessibility model, and picture them on Figure 8. Note that the sum of the vertical axis is always 1 due to the normalization. Obviously, different sequence positions and different convolution kernels have different weights, which proves SFA’s ability to regulate features.

In general, SFA and SFC make training smoother, faster, and better. They are simple but effective. Ac-

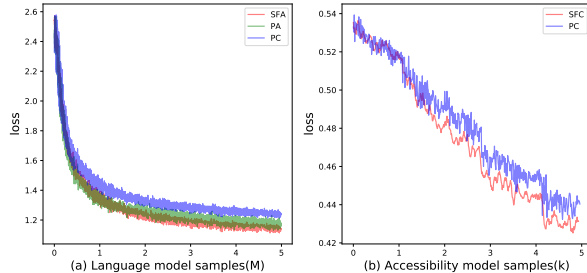


Figure 7: Loss in training time. **(a)** The loss curve for SFA, PA and PC in the training of DNA language model. **(b)** The loss curve for SFC and PC in the training of chromatin accessibility model.

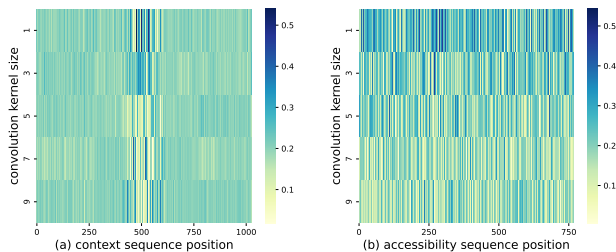


Figure 8: SFA and SFC parameters. **(a)** Parameters of SFA in the DNA language model. **(b)** Parameters of SFC in the chromatin accessibility model. Different sequence positions and different convolution kernels have different weights, which proves SFA’s ability to regulate features.

tually, since they share the same essence (Hadamard product), they share the same advantages.

5 Conclusion

In this article, we propose a chromatin accessibility prediction model named SemanticCAP. Our model is able to predict open regions of DNA, thus having a guiding role in disease detection, drug design, etc. For example, a gene called *CYMC* from cell H1-hESC mutated in the middle with a length of 5 bp, and its accessibility decreased from 0.98 to 0.14 predicted by our model, which is consistent with the experimental data that it reduces transcription (Klenova et al., 1993). Another example is a mutation in a gene called *HNF4A* from cell K562, which leads to a reduction in gene expression (Ellard and Colclough, 2006). Our model predicted that its accessibility decreased from 0.66 to 0.2, which gives a reasonable explanation for the experimental phenomenon of reduction in gene expression caused by the mutation. Similarly, we can monitor the accessibility changes of DNA targeted by drugs (especially anticancer drugs), and the change of accessibility will provide guidance for drug action.

The innovations of our method are as follows. First, we introduce the concept of language models in natural language processing to model DNA sequences. This method not only provides the word vector presentation of the base itself, but also provides sufficient information about the context of a site in a DNA sequence. Second, we use a small number of parameters to solve the feature fusion problem between different distributions. Specifically, we solve the problem of smooth addition of same dimensional distributions using SFA and the problem of smooth concat of different dimensional distributions using SFC. Third, we use an end-to-end model design, in which we fully utilize the learning ability and characteristics of the convolution and attention mechanism, thus achieving a better result with fewer parameters and shorter training time.

Of course, there is still much room for improvement in our method. In terms of the sample construction, we randomly select the same number of DNA sequences with the same length as negative samples. This approach may be modified. For example, we can deliberately use an unbalanced dataset, for there are so much DNA data, and then use some strategies such as ensemble learning (Dietterich et al., 2002) to eliminate the negative effects of data imbalance (Chawla and Sylvester, 2007). In terms of data input, sequence truncation or sequence completion operations exist in our model, which may cause information loss or redundant calculation. Also, the task we designed for the DNA language model could be enhanced. Multiple positions can be predicted simultaneously, just like the cloze problem in Bert. There are many other potential improvements. First is that the attention mechanism consumes too much memory, which could be replaced by a short-range attention or a mixed-length attention (Choromanski et al., 2020). Also, our smooth feature fusion method SFA and SFC could also be used in the multi-head attention to save space and accelerate training. Additionally, the dropout mechanism makes all neurons effective in the prediction phase, but there may exist a more reasonable way of fusing sub-networks. These issues need to be further explored.

Acknowledgement

This work was supported by the following: the National Natural Science Foundation of China (31801108, 62002251); the Natural Science Foundation of Jiangsu Province Youth Fund (BK20200856); and A Project Funded by the Priority Academic Program Development of Jiangsu Higher Education Institutions (PAPD). This work was partially supported by the Collaborative Innovation Center

of Novel Software Technology and Industrialization. The authors would also like to thank the support of Jiangsu Province Key Lab for providing information processing technologies.

References

- Aleksić, M. and Kapetanović, V. (2014). An overview of the optical and electrochemical methods for detection of dna-drug interactions. *Acta Chimica Slovenica* 61, 555–573
- Alipanahi, B., Delong, A., Weirauch, M. T., and Frey, B. J. (2015). Predicting the sequence specificities of dna-and rna-binding proteins by deep learning. *Nature biotechnology* 33, 831–838
- Ba, J. L., Kiros, J. R., and Hinton, G. E. (2016). Layer normalization. *arXiv preprint arXiv:1607.06450*
- Baldi, P. and Sadowski, P. J. (2013). Understanding dropout. *Advances in neural information processing systems* 26, 2814–2822
- Beer, M. A. (2017). Predicting enhancer activity and variant impact using gkm-svm. *Human mutation* 38, 1251–1258
- Bengio, Y., Courville, A., and Vincent, P. (2013). Representation learning: A review and new perspectives. *IEEE transactions on pattern analysis and machine intelligence* 35, 1798–1828
- Buenrostro, J. D., Wu, B., Chang, H. Y., and Greenleaf, W. J. (2015). Atac-seq: a method for assaying chromatin accessibility genome-wide. *Current protocols in molecular biology* 109, 21–29
- Chawla, N. V. and Sylvester, J. (2007). Exploiting diversity in ensembles: Improving the performance on unbalanced datasets. In *International Workshop on Multiple Classifier Systems* (Springer), 397–406
- Choromanski, K., Likhoshervostov, V., Dohan, D., Song, X., Gane, A., Sarlos, T., et al. (2020). Rethinking attention with performers. *arXiv preprint arXiv:2009.14794*
- de Ruijter, A. and Guldenmund, F. (2016). The bowtie method: A review. *Safety science* 88, 211–218
- Devlin, J., Chang, M.-W., Lee, K., and Toutanova, K. (2018). Bert: Pre-training of deep bidirectional transformers for language understanding. *arXiv preprint arXiv:1810.04805*
- Dietterich, T. G. et al. (2002). Ensemble learning. *The handbook of brain theory and neural networks* 2, 110–125
- Ellard, S. and Colclough, K. (2006). Mutations in the genes encoding the transcription factors hepatocyte nuclear factor 1 alpha (hnf1a) and 4 alpha (hnf4a) in maturity-onset diabetes of the young. *Human mutation* 27, 854–869
- Gallon, J., Loomis, E., Curry, E., Martin, N., Brody, L., Garner, I., et al. (2021). Chromatin accessibility changes at intergenic regions are associated with ovarian cancer drug resistance. *Clinical epigenetics* 13, 1–15
- Ghandi, M., Lee, D., Mohammad-Noori, M., and Beer, M. A. (2014). Enhanced regulatory sequence prediction using gapped k-mer features. *PLoS computational biology* 10, e1003711
- Giné, E. (1983). The lévy-lindeberg central limit theorem. *Proceedings of the American Mathematical Society* 88, 147–153
- Guo, Y., Zhou, D., Nie, R., Ruan, X., and Li, W. (2020). Deepanf: A deep attentive neural framework with distributed representation for chromatin accessibility prediction. *Neurocomputing* 379, 305–318
- Hochreiter, S. and Schmidhuber, J. (1997). Long short-term memory. *Neural computation* 9, 1735–1780
- Horn, R. A. (1990). The hadamard product. In *Proc. Symp. Appl. Math.* vol. 40, 87–169
- Huang, G., Liu, Z., Van Der Maaten, L., and Weinberger, K. Q. (2017). Densely connected convolutional networks. In *Proceedings of the IEEE conference on computer vision and pattern recognition*. 4700–4708
- Janssen, S., Cuvier, O., Müller, M., and Laemmli, U. K. (2000). Specific gain-and loss-of-function phenotypes induced by satellite-specific dna-binding drugs fed to drosophila melanogaster. *Molecular cell* 6, 1013–1024
- John, S., Sabo, P. J., Thurman, R. E., Sung, M.-H., Biddie, S. C., Johnson, T. A., et al. (2011). Chromatin accessibility pre-determines glucocorticoid receptor binding patterns. *Nature genetics* 43, 264–268
- Kalchbrenner, N., Grefenstette, E., and Blunsom, P. (2014). A convolutional neural network for modelling sentences. *arXiv preprint arXiv:1404.2188*

- Klenova, E., Nicolas, R., Paterson, H., Carne, A., Heath, C., Goodwin, G., et al. (1993). Ctf, a conserved nuclear factor required for optimal transcriptional activity of the chicken c-myc gene, is an 11-zn-finger protein differentially expressed in multiple forms. *Molecular and cellular biology* 13, 7612–7624
- Kumar, S. and Bucher, P. (2016). Predicting transcription factor site occupancy using dna sequence intrinsic and cell-type specific chromatin features. In *BMC bioinformatics* (Springer), vol. 17, 41–50
- Lee, D., Karchin, R., and Beer, M. A. (2011). Discriminative prediction of mammalian enhancers from dna sequence. *Genome research* 21, 2167–2180
- Liu, F. and Perez, J. (2017). Gated end-to-end memory networks. In *Proceedings of the 15th Conference of the European Chapter of the Association for Computational Linguistics: Volume 1, Long Papers*. 1–10
- Liu, Q., Xia, F., Yin, Q., and Jiang, R. (2018). Chromatin accessibility prediction via a hybrid deep convolutional neural network. *Bioinformatics* 34, 732–738
- Min, X., Zeng, W., Chen, N., Chen, T., and Jiang, R. (2017). Chromatin accessibility prediction via convolutional long short-term memory networks with k-mer embedding. *Bioinformatics* 33, i92–i101
- Pan, B., Kusko, R., Xiao, W., Zheng, Y., Liu, Z., Xiao, C., et al. (2019). Similarities and differences between variants called with human reference genome hg19 or hg38. *BMC bioinformatics* 20, 17–29
- Pennington, J., Socher, R., and Manning, C. D. (2014). Glove: Global vectors for word representation. In *Proceedings of the 2014 conference on empirical methods in natural language processing (EMNLP)*. 1532–1543
- Simon, J. M., Giresi, P. G., Davis, I. J., and Lieb, J. D. (2012). Using formaldehyde-assisted isolation of regulatory elements (faire) to isolate active regulatory dna. *Nature protocols* 7, 256–267
- Song, L. and Crawford, G. E. (2010). Dnase-seq: a high-resolution technique for mapping active gene regulatory elements across the genome from mammalian cells. *Cold Spring Harbor Protocols* 2010, pdb-prot5384
- Sun, C., Yang, Z., Luo, L., Wang, L., Zhang, Y., Lin, H., et al. (2019). A deep learning approach with deep contextualized word representations for chemical–protein interaction extraction from biomedical literature. *IEEE Access* 7, 151034–151046
- Vaswani, A., Shazeer, N., Parmar, N., Uszkoreit, J., Jones, L., Gomez, A. N., et al. (2017). Attention is all you need. In *Advances in neural information processing systems*. 5998–6008
- Wang, Y., Jiang, R., and Wong, W. H. (2016). Modeling the causal regulatory network by integrating chromatin accessibility and transcriptome data. *National science review* 3, 240–251
- Xu, Y. and Strick, A. J. (2021). Integration of unpaired single-cell chromatin accessibility and gene expression data via adversarial learning. *arXiv preprint arXiv:2104.12320*
- Zhou, J. and Troyanskaya, O. G. (2015). Predicting effects of noncoding variants with deep learning-based sequence model. *Nature methods* 12, 931–934